Allosteric Coupling between the Lid and Interdomain Linker in DnaK Revealed by Inhibitor Binding Studies

Article *in* Journal of bacteriology · March 2009

DOI: 10.1128/JB.01131-08 · Source: PubMed

CITATIONS
53

READS
55

2 authors:

Markus Liebscher
Scil Proteins Gmbh
4 PUBLICATIONS **104** CITATIONS
SEE PROFILE

Anna Roujeinikova
Monash University (Australia)
95 PUBLICATIONS **1,919** CITATIONS
SEE PROFILE

Journal of Bacteriology

Allosteric Coupling between the Lid and Interdomain Linker in DnaK Revealed by Inhibitor Binding Studies

Markus Liebscher and Anna Roujeinikova
J. Bacteriol. **2009, 191(5):1456. DOI: 10.1128/JB.01131-08.**
Published Ahead of Print 19 December 2008.

JOURNAL OF BACTERIOLOGY, Mar. 2009, p. 1456–1462 Vol. 191, No. 5
0021-9193/09/$08.00+0 doi:10.1128/JB.01131-08

Allosteric Coupling between the Lid and Interdomain Linker in DnaK Revealed by Inhibitor Binding Studies▽

Markus Liebscher[1] and Anna Roujeinikova[2]*

Biocenter, Martin Luther University Halle-Wittenberg, Weinbergweg 22, D-06120 Halle (Saale), Germany,[1] and Manchester Interdisciplinary Biocenter, Faculty of Life Sciences, University of Manchester, 131 Princess Street, Manchester M1 7DN, United Kingdom[2]

Received 12 August 2008/Accepted 10 December 2008

The molecular chaperone DnaK assists protein folding and refolding, translocation across membranes, and regulation of the heat shock response. In *Escherichia coli*, the protein is a target for insect-derived antimicrobial peptides, pyrrhocoricins. We present here the X-ray crystallographic analysis of the *E. coli* DnaK substrate-binding domain in complex with pyrrhocoricin-derived peptide inhibitors. The structures show that pyrrhocoricins act as site-specific, dual-mode (competitive and allosteric) inhibitors, occupying the substrate-binding tunnel and disrupting the latch between the lid and the β-sandwich. Our structural analysis revealed an allosteric coupling between the movements of the lid and the interdomain linker, identifying a previously unknown mechanism of the lid-mediated regulation of the chaperone cycle.

DnaK is the bacterial molecular chaperone from the Hsp70 (70-kDa heat shock protein) family that assists many cellular processes involving proteins in their nonnative conformations, such as folding of newly synthesized proteins, protein translocation across membranes, refolding of misfolded and aggregated proteins, degradation of unstable proteins, and regulation of the heat shock response (for reviews, see references 10, 28, and 42). The chaperone function of DnaK is based on its ability to transiently bind to exposed stretches of hydrophobic residues in partially or fully unfolded proteins in an ATP-controlled fashion, thereby preventing aggregation and misfolding. DnaK recognizes short peptide sequences containing up to five consecutive hydrophobic residues (with leucine found frequently in the middle), flanked preferentially by basic residues (42, 43). The molecular-chaperone activity is functionally linked with ATP hydrolysis; the substrate-binding and release cycle is driven by the switching between the ATP-bound state, with low affinity and a high exchange rate for substrates, and the ADP-bound state, with high affinity and a low exchange rate for substrates.

In vivo, DnaK activity is supported by two cochaperones, GrpE, which facilitates the ADP/ATP exchange, and DnaJ, which stimulates ATP hydrolysis and thus aids the peptide capture (10, 25, 28, 38, 54). DnaJ itself also recognizes exposed stretches of hydrophobic residues in partially unfolded or denatured proteins, with specificity overlapping with that of DnaK (44). It is therefore thought that DnaJ serves as a scanning factor for DnaK by binding specific unfolded substrates and presenting them to the ATP-bound form of DnaK.

Escherichia coli DnaK is composed of two domains: an N-terminal ATPase domain (residues 1 to 387) and a C-terminal substrate-binding domain (SBD) (residues 388 to 638) (10). The latter is made up of an 18-kDa β-sandwich subdomain that holds the substrate-binding cleft and a C-terminal α-helical-bundle "lid" subdomain that stabilizes the complex with the peptide substrate and controls the accessibility of the peptide binding site but does not interact with the substrate directly (5, 55). Removal of the lid subdomain by truncation decreases the affinity of DnaK for polypeptide substrates, primarily by increasing the dissociation rates (9, 28, 46, 47).

The activities of the ATPase and the SBDs are allosterically coupled. ATP binding induces a global conformational change that results in the docking of the ATPase domain onto the SBD and opening of the latter, thus triggering the release of a peptide substrate (45, 46). Peptide binding, in turn, accelerates DnaK/DnaJ-mediated ATP hydrolysis, followed by trapping of the substrate and dissociation of the ATPase domain from the SBD. Upon the subsequent GrpE-mediated exchange of ADP for ATP, DnaK returns to the beginning of its molecular-chaperone cycle (references 6 and 28 and references therein). In this manner, DnaK alternates between the "open" (low-peptide-affinity) and closed (high-peptide-affinity) states. The detailed molecular mechanism of the allosteric interdomain communication is unknown, although the previous mutagenesis studies identified the conserved interdomain linker VLLL (389 to 392) (25), the segment 507 to 537 (32), and residue K414 (31) on the SBD surface as the structural elements that are required for signal transmission.

Previous X-ray crystallographic and nuclear magnetic resonance studies of the SBD complex with the heptapeptide NR (NRLLLTG) provided an insight into the structural basis for the substrate recognition and amino acid sequence specificity of DnaK (48, 55). The peptide has been shown to bind in a short tunnel formed by the loops of the β-sandwich subdomain of the SBD in an extended conformation through hydrophobic and van der Waals side chain interactions and hydrogen bonds between the peptide backbones of the substrate and the SBD. These structures rationalized the ability of DnaK to differentiate between native and nonnative protein conformers by recognizing struc-

* Corresponding author. Mailing address: Manchester Interdisciplinary Biocenter, Faculty of Life Sciences, University of Manchester, 131 Princess St., Manchester M1 7DN, United Kingdom. Phone: 44 161 3065155. Fax: 44 161 3065201. E-mail: Anna.Roujeinikova@manchester.ac.uk.

▽ Published ahead of print on 19 December 2008.

TABLE 1. X-ray data collection statistics

Parameter	Value[b]		
	Short-peptide complex form A	Long-peptide complex form:	
		A	B
Wavelength (Å)	1.00	1.54	1.00
Resolution range (Å)	80–2.1 (2.21–2.10)	15–2.5 (2.59–2.50)	10–2.6 (2.74–2.60)
Completeness (%)	98 (98)	88 (93)	82 (87)
No. of observed reflections	110,817	46,703	154,544
No. of unique reflections	32942	17463	27880
Avg $I/\sigma I$	9.7 (3.7)	3.8 (1.8)	20.7 (13.2)
R_{merge}[a]	0.090 (0.318)	0.127 (0.371)	0.067 (0.117)

[a] $R_{merge} = \frac{\left(\sum_h \sum_i |I_{hi} - \langle I_h \rangle|\right)}{\sum_h \sum_i |I_{hi}|}$, where I_{hi} is the intensity of the ith observation of reflection h.

[b] The numbers in parentheses indicate the values for the highest-resolution shell.

tural features common to nascent chains: an accessible peptide backbone and solvent-exposed aliphatic side chains.

DnaK has been identified as a molecular target of pyrrhocoricin (L-PYR) (VDKGSYLPRPTPPRPIYNRN), an insect-derived antibacterial peptide (13, 23, 34). Nontoxicity to mammalian cells and good serum stability of L-PYR-derived peptides make them promising drug candidates in treating emerging/re-emerging antimicrobial-resistant bacterial pathogens (15, 35) and highlight the importance of detailed structural characterization of inhibitor-protein interactions with a view to rational drug design. This paper describes the first crystal structures of the *E. coli* DnaK SBD, truncated at the C terminus (residues 389 to 607), in complex with two L-PYR-derived peptidic inhibitors, one of which (the short peptide) displays nanomolar affinity for nucleotide-free *E. coli* DnaK (K_d [dissociation constant] = 5.5 nM, the lowest that has ever been reported for any peptide [M. Liebscher, unpublished data]).

MATERIALS AND METHODS

Crystallization and data collection. The SBD of *E. coli* DnaK (residues 389 to 607) was expressed in *E. coli* and purified by following the previously described protocol (55). The synthetic peptides used were Val-Asp-Lys-Leu-Tyr-Cha-Leu-Pro-Arg-Pro-Thr-Pro-Pro-Arg-Pro-Ile-Tyr-Asn-Arg-Asn (referred to as the long peptide) and Val-Asp-Lys-Leu-Tyr-Cha-Leu-Pro-Arg-Pro-Thr (the short peptide); Cha stands for D-cyclohexylalanine. Solid-phase peptide synthesis was performed on the Syro II multiple-peptide synthesizer (MultiSynTech) using standard 9-fluorenylmethoxy carbonyl protection chemistry. The lyophilized peptides were dissolved at 100 mM in 20 mM Tris, pH 8.0. Prior to crystallization, the protein solution in 20 mM Tris, pH 8.0, was concentrated to 15 mg/ml; mixed with the peptide solution at 5:1 and 0.5:1 molar ratios for the short and long peptides, respectively; incubated at room temperature for 1 h; and cleared by centrifugation for 20 min at 13,000 × *g*.

The crystal of the *E. coli* DnaK SBD complex with the short peptide was obtained using the sitting-drop vapor diffusion method, with 2.4 M ammonium sulfate and 100 mM citric acid, pH 5.0, as a reservoir solution. The crystal belongs to space group $P2_12_12$ with unit cell dimensions of 77.6 (a), 160.0 (b), and 44.9 (c) Å and with two protein molecules in the asymmetric unit. Diffraction data for this crystal were collected to 2.1-Å resolution on the European Synchrotron Radiation Facility beam line ID23-1 (Grenoble, France). The data were processed and scaled using the programs MOSFLM (26) and SCALA (14).

Cocrystallization of the *E. coli* DnaK SBD with the long peptide using 2.4 M ammonium sulfate, 100 mM citric acid (pH 4.0 to 5.0) as a reservoir solution in a sitting-drop vapor diffusion setup yielded two different but related crystal forms. Crystals of one form (hereafter referred to as form A) belong to space group $P2_12_12$ with unit-cell dimensions of 77.9 (a), 159.1 (b), and 44.8 (c) Å and are isomorphous with those of the complex with the short peptide. Form B crystals belong to space group $P2_12_12_1$ with unit-cell dimensions of 77.7 (a), 91.7 (b), and 154.8 (c) Å and with four monomers in the asymmetric unit.

The X-ray data set for the cryocooled form A crystal of the complex with the long peptide was collected to 2.5-Å resolution using a Rigaku MicroMax007 microfocus rotating anode generator, a Rigaku Raxis-IV imaging plate area detector, and an X-Stream 2000 cold-stream generator. This data set was processed and scaled using d*TREK (37). Diffraction data for the form B crystal of this complex were collected to 2.6-Å resolution on the European Synchrotron Radiation Facility beam line ID14-4 and processed using MOSFLM and SCALA. Data in the low-resolution shell of this set had substantial rejections owing to oversaturation and were excluded from merging and refinement due to low completeness. The statistics of all data collection are summarized in Table 1.

Structure determination and refinement. The crystal structure of the *E. coli* DnaK SBD complex with the short peptide was determined using molecular replacement (the Phaser program [30]), with the structure of the *E. coli* DnaK SBD complexed with the NR heptapeptide (Protein Data Bank [PDB] entry 1dkx) (55) as the starting model. The difference Fourier maps clearly showed substantially different positions for the helical-lid domain (residues 536 to 607), which rotated by 9° in one monomer and by 30° in the second monomer about the hinge axis passing through residue 533. The lid domains were placed into their new positions using Molrep (51) and an ($F_{obs} - F_{calc}$) difference electron density map calculated including β-sandwich domains only. The structure was then rebuilt where necessary using Coot (17) in combination with restrained positional and isotropic *B*-factor refinement using Refmac (14). The subsequent difference Fourier maps showed the positions of residues 3 to 11 of the peptide bound to the β-sandwich domain in both monomers. The inhibitor molecule was incorporated into the model, which was then subjected to alternating rounds of refinement and automatic water molecule search (36).

The structure of the form A *E. coli* DnaK SBD complex with the long peptide was solved simply by calculating the initial set of phases using the coordinates of the protein part of the refined short-peptide complex following the rigid-body refinement using data in the range [15 to 3.5 Å]. The difference Fourier maps showed the location of the inhibitor residues 3 to 11 in one protein monomer and 3 to 14 in the other. The inhibitor molecules were incorporated into the model, which was then subjected to rounds of restrained positional and isotropic *B*-factor refinement and automatic water molecule search (Refmac, ARP/wARP).

The structure of the form B crystal complex with the long peptide was solved using molecular replacement (Phaser) with the coordinates of the two protein monomers (A and B) of the short-peptide complex as a search model. The asymmetric unit of this form contains four protein molecules. The refinement statistics for all models are summarized in Table 2. Calculations of the protein surface area buried at the interface with the ligand were carried out using DSSP (14).

Determination of the binding constants. The binding constants were determined using the fluorescence-dependent competition assay, based on the procedure published by McCarty et al. (29). Briefly, 0.1 μM DnaK was preincubated in buffer (25 mM HEPES/KOH, pH 7.6, 50 mM KCl, 5 mM $MgCl_2$) at 30°C for 90 min with 0.5 μM σ^{32}-Q132-Q144-C-IAANS. The peptide was added in increasing amounts to the mixture and incubated each time for at least 30 min. Fluorescence emission at 460 nm was recorded (Hitachi F-3010) with excitation

TABLE 2. Refinement statistics

Parameter	Value		
	Short-peptide complex	Long-peptide complex form:	
		A	B
Resolution range (Å)	15–2.1	15–2.5	8–2.6
R factor*	0.178	0.237	0.254
Free R factor[a]	0.241	0.316	0.319
Bond length deviation from ideality (Å)	0.013	0.013	0.012
Bond angle deviation from ideality (degrees)	1.4	2.0	1.8
Avg B (protein atoms) (Å^2)	20	42	24
Avg B (water molecules) (Å^2)	33	41	26
Avg B (peptide inhibitor)[b] (Å^2)	24	45	29
DnaK residues included in the model	389–601 (chain A) 389–603 (B)	389–600 (chain A) 389–602 (B)	389–600 (chain A) 391–602 (B) 389–550, 560–600 (E) 389–602 (F)
Ramachandran plot[c]	96.5/3.5/0/0	88.6/10.4/1.0/0	82.5/16.3/1.2/0

[a] $R = \Sigma (F_{obs} - F_{calc}) / \Sigma (F_{obs})$.
[b] The free *R* factor was calculated on 5% of the data omitted at random.
[c] Percent most favored/additionally allowed/generously allowed/disallowed.

at 335 nm. The normalized data were used to calculate the K_d value according to the method of Wang (52).

Protein structure accession numbers. Coordinates and structure factors for the *E. coli* DnaK complexes with the short (form A) and the long (forms A and B) peptide inhibitors have been deposited in the PDB with accession numbers 3DPO, 3DPP, and 3DPQ, respectively.

RESULTS AND DISCUSSION

Overall fold and localization of the inhibitor binding site. The crystal structures of the *E. coli* DnaK SBD complexed with the short and the long L-PYR-derived inhibitor peptides were determined using molecular replacement with the structure of the *E. coli* DnaK SBD complexed with the NR heptapeptide (55). The overall fold of the β-sandwich and the helical-bundle subdomains was found to be essentially the same as that observed for the NR complex. The relative value of the protein accessible surface area shielded by the intermolecular contacts in the two observed crystal forms did not exceed 4%, indicating that the protein is monomeric in the crystal. This finding is consistent with the results of the previous biochemical and biophysical studies that demonstrated that the β-sandwich subdomain, SBD, and full-length DnaK and the other Hsp70 proteins are monomeric in the peptide-bound form (2, 3, 4, 6, 19, 21, 45, 48).

The electron density maps (Fig. 1A) clearly revealed the almost identical modes of binding of the short and the long peptides in the substrate-binding tunnel of the β-sandwich subdomain (Fig. 1B). The N-terminal 2 residues of the peptides were not seen in the density maps, possibly due to the lack of stabilizing interactions with the protein. Structural analysis revealed that both the short and the long peptides contact the SBD via residues 4 to 10 (LYChaLPRP). The 9-residue C-terminal extension of the long peptide does not form additional interactions with the same protein molecule; instead, it is stabilized by the contacts with the symmetry-related monomer, with residues 11 to 14 being visible in the electron density map. The details of the interaction of the peptide inhibitor with the SBD are therefore described below for the short-peptide complex.

The short peptide binds in an extended conformation that is stabilized by six direct and one water-mediated hydrogen bonds to the peptide main chain and multiple van der Waals contacts with its side chains (Fig. 1C). Leu4 and Tyr5 side chains remain largely solvent exposed, making van der Waals contacts with the main-chain peptide of Val425 and the side chain of Phe426, respectively. The cyclohexyl ring of Cha6 is buried in the pocket formed by the side chain of His541 and the main-chain fragment 427 to 428. The side chain of Leu7 is in a strongly hydrophobic environment, surrounded by the side chains of Phe426, Val436, and Ile438. Pro8 forms van der Waals contacts with the side chains of Glu402 and Val436 and with the main-chain peptide of Thr437. Arg9 is largely solvent exposed, making a single van der Waals contact with the main-chain peptide of Ala435. Pro10 binds to a surface patch formed by the stretch 435 to 437 and Asn458.

The differences between the sequences of the inhibitor peptides in this study and L-PYR are limited to substitution of LYCha by GSY. This strongly suggests that L-PYR is likely to bind to the DnaK SBD via its residues 4 to 10 in a manner very similar to that seen in the crystal structures of the short- and long-peptide complexes. The previous report identifying Asp2-Pro10 as an active motif of L-PYR further supports this view (24).

It had been previously suggested that DnaK may have two binding sites for L-PYR, the substrate-binding site and the hinge region between helices D and E (23, 24, 34). This proposal was later disputed by Chesnokova and coworkers (12), who presented kinetic data that were consistent with a single binding site in the substrate channel. Our analysis of the complexes of SBD with the L-PYR-derived peptides in two different crystal forms also shows no indication of the aforementioned second binding site near the D-E region.

L-PYR-like peptides act as competitive inhibitors. Superimposition of the crystal structures of the *E. coli* SBD complexes with the short L-PYR-derived peptide and with the NR peptide (55) over the Cα atoms of the β-sandwich subdomain revealed the very close overall similarity of the peptide binding mode (Fig. 1D). This suggests that inhibitory properties of the L-

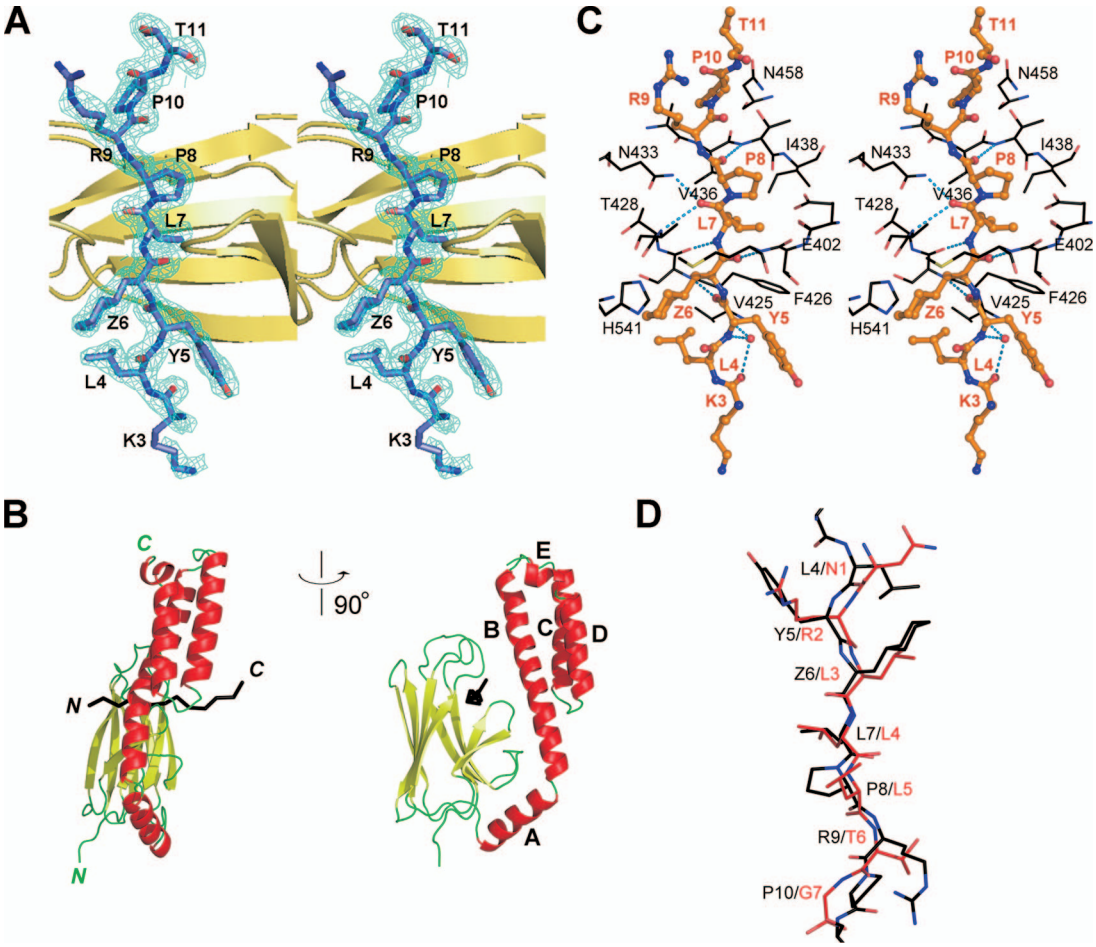

FIG. 1. Inhibitor binding to the DnaK SBD. (A) Stereoview of the electron density for the short L-PYR-derived peptide bound to the *E. coli* DnaK SBD. The ($2mF_o$-DF_c) sigma A-weighted (41) map was calculated at 2.1-Å resolution and contoured at one σ level. (B) Schematic cartoon of the SBD complex with the short peptide. (C) Stereoview illustrating the interactions between the short peptide (drawn in ball-and-stick representation with carbons in brown) and the DnaK SBD. (D) Superposition of the short peptide (with carbons in black) and the NR peptide bound to SBD in their respective complexes, showing the peptide conformations (the protein part is omitted).

PYR-like peptides can be partly explained by the fact that they compete with natural peptide substrates for the same binding site. The binding affinity of the short peptide to nucleotide-free DnaK (K_d = 5.5 nM) exceeds that of the NR peptide by at least 50-fold (39). In order to obtain the molecular explanation for the improved binding, a detailed comparative analysis of the crystal structures of the SBD/NR and SBD/short-peptide complexes was performed. Comparative structure analysis revealed that the protein-inhibitor interactions involve seven consecutive residues (residues 4 to 10) of the latter, whereas the interactions in the NR complex engage only the five middle residues (RLLLT) of the peptide. In the NR complex, the polar side chain of the N-terminal asparagine of the peptide points into the solvent, while in the inhibitor complex, the aliphatic side chain of the equivalent residue (Leu4) packs against the protein surface. At the C-terminal exit from the substrate-binding channel, the terminal glycine of the NR peptide forms no contacts with the protein. The substitution of this residue by proline in the inhibitor complex provides additional side chain-mediated stabilizing interactions with the protein. In agreement with these observations, the calculations of the protein surface area buried at the interface with the inhibitor gave a value that was 10% higher for the NR complex (494 versus 446 Å^2).

In conclusion, the crystal structures of the *E. coli* DnaK SBD complexes with L-PYR-derived peptides reveal that the inhibitor binds in the conventional peptide binding site of SBD, mimicking natural substrates. This finding is consistent with the previous observation that the k_{on} and k_{off} values (association and dissociation rate constants, respectively) for the L-PYR binding to low-affinity DnaK (ATP-DnaK) are close to the kinetic constants for short synthetic peptides that bind to the conventional substrate-binding site of DnaK (12). Altogether, this suggests that L-PYR antimicrobial activity is at least partly due to the competitive inhibition of the refolding activity of DnaK. Taking into consideration the prominent sequence variation of Hsp70s in the SBD (7), the crystal structures presented provide a useful foundation for the rational design of more effective or species-specific L-PYR-like peptide or peptidomimetic antimicrobial drugs.

Allosteric mechanism of inhibition. The detailed comparative analysis of the protein-ligand contacts in the crystals of the

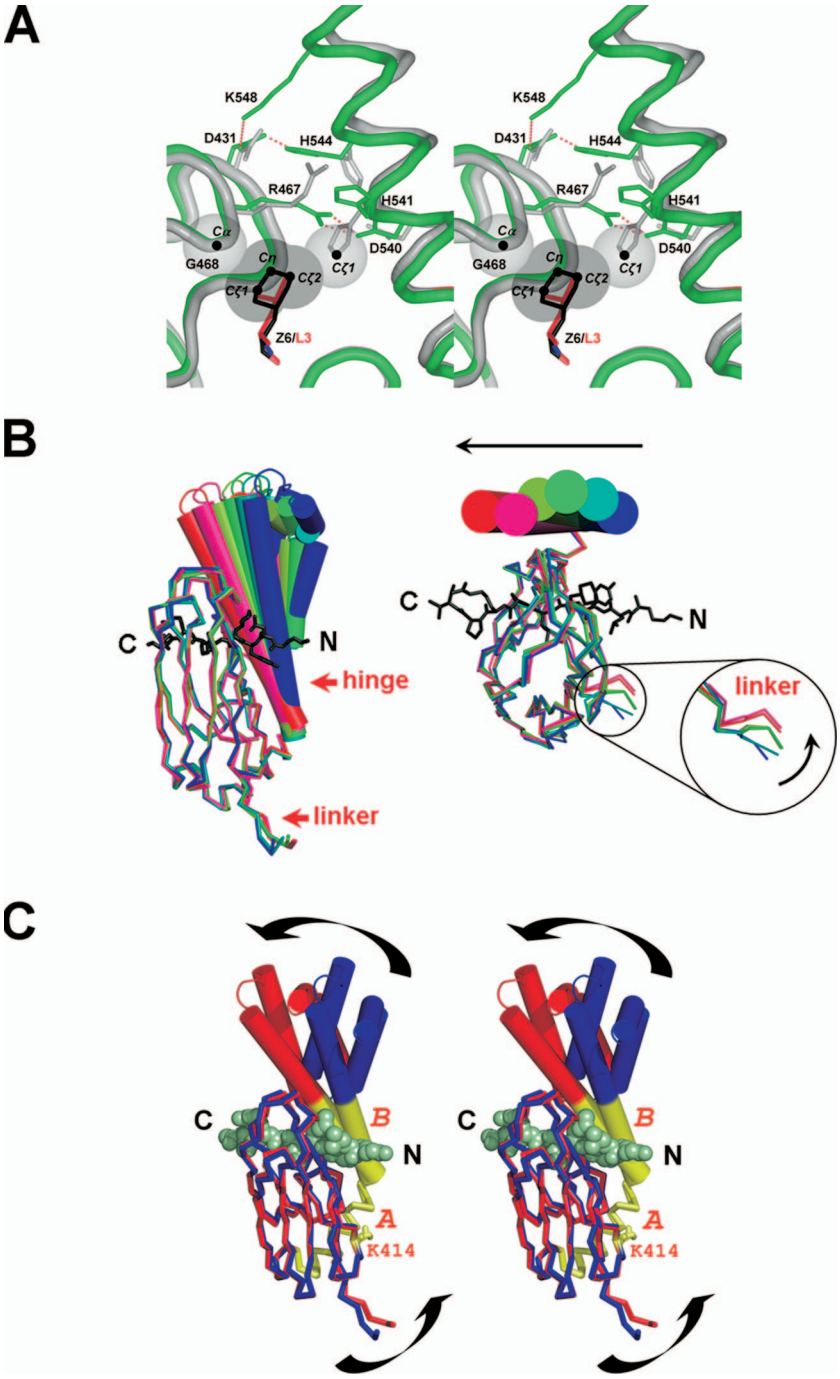

FIG. 2. Allosteric link between the lid and the interdomain linker. (A) Superposition of the short peptide (with carbons in black) and the NR peptide (red) bound to the SBD in their respective complexes, showing the broken latch and the additional hydrophobic contacts stabilizing Cha. The protein moiety is shown in gray for the short-peptide complex and in green for the NR peptide complex. (B) Superimposition of the representative structures showing variation in the angle of packing of the helical-lid subdomain against the β-sandwich; shown are a side view (left) and a top view (right). The structure PDB accession number 1dkx (SBD/NR) is shown in blue; chains A and B of the SBD/short-peptide complex are in dark green and red, respectively; chain A of PDB accession number 1dky is in light blue; and chains A and F of the form B long-peptide complex are in light green and pink, respectively. (C) The coupled motions of the lid and the linker with respect to the docking site for the ATPase domain (yellow).

short- and the two different forms of the long-peptide inhibitor complexes and that of the SBD/NR complex (PDB accession number 1dkx) (55) was carried out by superimposing the structures over their respective β-subdomains. The analysis suggests that introduction of a bulky aliphatic cyclohexylalanine side chain at the position of Leu3 in the NR peptide induces a conformational rearrangement in the protein that creates a more hydrophobic environment for the former (Fig. 2A). The

charged side chain of Arg467 turns away, with a concomitant torsional shift in His544 to accommodate it. The side chain of His541 rotates toward the Cha, and the loop harboring Arg467 shifts in the Cha direction, providing additional stabilizing hydrophobic contacts between His541 CE1 and Cha CE2 and between Gly468 CA and Cha CE1 and CZ.

As a result of these rearrangements, the so called "latch" between the β-sandwich and the helical-lid subdomains, observed in the NR complex (55) and comprising hydrogen bonds Arg467-Asp540 and Asp431-His544 and salt bridge Asp431-Lys548 (Fig. 2A), is broken in all inhibitor-bound molecules. Previous site-directed mutagenesis studies demonstrated the functional importance of the ionic interactions at the "latch." Removal of the Arg467-Asp540 and Asp431-Lys548 bridges by the double D540A/K548A mutation rendered DnaK inactive in a luciferase-refolding assay in the presence of GrpE and DnaJ (18), most likely by affecting its ability to interact with DnaJ (1). The substitution of Arg469 in rat Hsc70 (equivalent to Arg467 in DnaK) by cysteine produces a variant that has an impaired refolding activity (11). Disruption of the latch between the β-sandwich and the helical-lid subdomains by the inhibitor binding in the substrate tunnel is therefore likely to affect the refolding DnaK activity in a similar way. Thus, the structural analysis of the crystal DnaK SBD complexes with the short and long inhibitor peptides strongly suggests that, in addition to the competitive inhibition, an allosteric inhibition takes places.

Large-scale movement of the helical-lid subdomain. Structure comparisons of the inhibitor-bound SBD molecules in the crystals of two different forms and the previously reported crystal structures of the SBD/NR complex (PDB accession numbers 1dkx, 1dky, and 1dkz) (55) revealed significant conformational variations. Structure superpositions and a DynDom analysis of the domain dynamics (22) showed that these variations are due to the difference in the angle of packing of the helical bundle comprising residues 540 to 607 (the C-terminal half of helix B and helices C to E) against the β-sandwich (Fig. 2B and C). Our analysis suggests that the helical-lid subdomain can swing about the hinge, located at residues 525 to 540 (as determined by the DynDom analysis), by as much as 30°. The structures of the separate β-sandwich and the helical-lid domains, and the mode of the peptide binding, are essentially identical in all conformers, suggesting that the two subdomains of SBD move as rigid bodies. This is consistent with previous observations that, when expressed on their own, these domains form stably folded and quite rigid structures (5, 49). The two extreme positions of the helical lid in the observed spectrum of conformations are defined by the structures PDB accession number 1dkx (SBD/NR) and chain B of the SBD/short-peptide complex (Fig. 2B). The respective domain in the remaining set of structures under consideration occupies intermediate positions.

Allosteric coupling between the helical lid and interdomain linker. The comprehensive analysis of the spectrum of all available crystal structures of peptide-bound DnaK SBD (this study and PDB accession numbers 1dkx, 1dky, and 1dkz) (55) superimposed over their respective β-sandwich subdomains revealed a previously unobserved correlation between the positions of the helical lid and the N-terminal segment VLLL (389 to 392) of the SBD (the latter links the SBD and the ATPase domain in the full-length DnaK). As illustrated in Fig. 2B and C, rotation of the helical lid in the direction approximately parallel to the vector from the N to the C terminus of the bound peptide is accompanied by a shift of the interdomain linker in the direction toward helix A. To exclude the possibility that this was a crystal-packing artifact, the structures of all distinct conformers in four different crystal forms (form A and form B [this study] and form 1 and form 2 [55]) were included in this analysis; the results consistently showed that the two extreme positions observed for the helical lid correspond to the two extreme positions seen for the linker, and the intermediate lid positions correspond to the intermediate positions of the linker. This correlation reveals, for the first time, an allosteric coupling between the movements of the helical lid and the interdomain linker, which is mediated by subtle changes in the structure of the β-sandwich subdomain.

This discovery has important functional implications. The spatial arrangement of the ATPase domain and the SBD, connected by the linker, changes significantly between the ADP- and ATP-bound states. In the ADP-bound state, the two domains are in disjoined conformations and do not interact (49, 50). In the ATP-bound state, the ATPase domain docks onto the SBD, inducing concerted conformational changes in both the β-sandwich and helical-lid subdomains of the SBD (8, 33, 50). The docking site for the ATPase domain (helix A; the N-terminal half of helix B, including the hinge [32]; and Lys414 [31]) is shown in Fig. 2C. Our structural analysis therefore suggests that in the full-length DnaK, the shift of the interdomain linker in the direction toward helix A, concomitant with the rotation of the helical lid in the direction of the C terminus of the bound peptide, would occur on the approach of the two domains for docking. Recent kinetic measurements of the ATP-induced quenching of Trp102 suggested that docking of the ATP-bound ATPase domain onto the SBD is gated by the lid (46, 47). Our observation that the twist of the linker upon the domain's approach is allosterically coupled with the disruption of the latch and rotation of the helical lid provides the molecular explanation of this gating phenomenon.

The reverse movement of the lid subdomain, in the direction toward the N terminus of the bound substrate, would be accompanied by the shift of the linker away from the docking surface, thus facilitating dissociation of the two domains. Our finding therefore suggests that the lid movement can allosterically regulate association/dissociation of the two domains. The C-terminal tail of the lid subdomain has been implicated in interactions of mammalian Hsp70s with DnaJ homologues (16, 20, 27, 40, 53). Allosteric regulation of the association of the ATPase domain and the SBD by the lid movement is therefore likely to play an important functional role in the operation of the DnaK-DnaJ chaperone machine.

ACKNOWLEDGMENTS

We thank Andrew McCarthy and Hassan Belrhali at the European Synchrotron Radiation Facility (Grenoble, France) and Patrick Bryant at the X-Ray Crystallography Facility (University of Manchester) for assistance with data collection.

A.R. is a Wellcome Trust Research Career Development Fellow.

REFERENCES

1. **Acebrón, S. P., V. Fernández-Sáiz, S. G. Taneva, F. Moro, and A. Muga.** 2008. DnaJ recruits DnaK to protein aggregates. J. Biol. Chem. **283:**1381–1390.

2. **Azem, A., W. Oppliger, A. Lustig, P. Jeno, B. Feifel, G. Schatz, and M. Horst.** 1997. The mitochondrial hsp70 chaperone system: effect of adenine nucleotides, peptide substrate, and mGrpE on the oligomeric state of mhsp70. J. Biol. Chem. **272:**20901–20906.
3. **Benaroudj, N., F. Triniolles, and M. M. Ladjimi.** 1996. Effect of nucleotides, peptides, and unfolded proteins on the self-association of the molecular chaperone HSC70. J. Biol. Chem. **271:**18471–18476.
4. **Benaroudj, N., B. Fouchaq, and M. M. Ladjimi.** 1997. The COOH-terminal peptide binding domain is essential for self association of the molecular chaperone HSC70. J. Biol. Chem. **272:**8744–8751.
5. **Bertelsen, E. B., H. Zhou, D. F. Lowry, G. C. Flynn, and F. W. Dahlquist.** 1999. Topology and dynamics of the 10 kDa C-terminal domain of DnaK in solution. Protein Sci. **8:**343–354.
6. **Blond-Elguindi, S., A. M. Fourie, J. F. Sambrook, and M.-J. H. Gething.** 1993. Peptide-dependent stimulation of the ATPase activity of the molecular chaperone BiP is the result of conversion of oligomers to active monomers. J. Biol. Chem. **268:**12730–12735.
7. **Boorstein, W. R., T. Ziegelhoffer, and E. A. Craig.** 1994. Molecular evolution of the HSP70 multigene family. J. Mol. Evol. **38:**1–17.
8. **Buchberger, A., H. Theyssen, H. Schröder, J. S. McCarty, G. Virgallita, P. Milkereit, J. Reinstein, and B. Bukau.** 1995. Nucleotide-induced conformational changes in the ATPase and substrate binding domains of the DnaK chaperone provide evidence for interdomain communication. J. Biol. Chem. **270:**16903–16910.
9. **Buczynski, G., S. V. Slepenkov, M. G. Sehorn, and S. N. Witt.** 2001. Characterization of a lidless form of the molecular chaperone DnaK. J. Biol. Chem. **276:**27231–27236.
10. **Bukau, B., and A. L. Horwich.** 1998. The Hsp70 and Hsp60 chaperone machines. Cell **92:**351–366.
11. **Chang, T.-C., C.-D. Hsiao, S.-J. Wu, and C. Wang.** 2001. The effect of mutating arginine-469 on the substrate binding and refolding activities of 70-kDa heat shock cognate protein. Arch. Biochem. Biophys. **386:**30–36.
12. **Chesnokova, L. S., S. V. Slepenkov, and S. N. Witt.** 2004. The insect antimicrobial peptide, L-pyrrhocoricin, binds to and stimulates the ATPase activity of both wild-type and lidless DnaK. FEBS Lett. **565:**65–69.
13. **Cociancich, S., A. Dupont, G. Hegy, R. Lanot, F. Holder, C. Hetru, J.-A. Hoffmann, and P. Bulet.** 1994. Novel inducible antibacterial peptide from a hemipteran insect, the sap-sucking bug *Pyrrhocoris aptarus*. Biochem. J. **300:** 567–575.
14. **Collaborative Computational Project No. 4.** 1994. The CCP4 suite: programs for protein crystallography. Acta Crystallogr. D **50:**760–763.
15. **Cudic, M., B. A. Condie, D. J. Weiner, E. S. Lysenko, Z. Q. Xiang, O. Insug, P. Bulet, and L. Otvos, Jr.** 2002. Development of novel antibacterial peptides that kill resistant clinical isolates. Peptides **23:**2071–2083.
16. **Demand, J., J. Luders, and J. Hohfeld.** 1998. The carboxy-terminal domain of Hsc70 provides binding sites for a distinct set of chaperone cofactors. Mol. Cell. Biol. **18:**2023–2028.
17. **Emsley, P., and K. Cowtan.** 2004. Coot: model-building tools for molecular graphics. Acta Crystallogr. D **60:**2126–2132.
18. **Fernández-Sáiz, V., F. Moro, J. M. Arizmendi, S. P. Acebrón, and A. Muga.** 2006. Ionic contacts at DnaK substrate binding domain involved in the allosteric regulation of lid dynamics. J. Biol. Chem. **281:**7479–7488.
19. **Fouchaq, B., N. Benaroudj, C. Ebel, and M. M. Ladjimi.** 1999. Oligomerization of the 17-kDa peptide-binding domain of the molecular chaperone HSC70. Eur. J. Biochem. **259:**379–384.
20. **Freeman, B. C., M. P. Myers, R. Schumacher, and R. I. Morimoto.** 1995. Identification of a regulatory motif in Hsp70 that affects ATPase activity, substrate binding and interaction with HDJ-1. EMBO J. **14:**2281–2292.
21. **Gao, B., E. Eisenberg, and L. Greene.** 1996. Effect of constitutive 70-kDa heat shock protein polymerization on its interaction with protein substrate. J. Biol. Chem. **271:**16792–16797.
22. **Hayward, S., and H. J. C. Berendsen.** 1998. Systematic analysis of domain motions in proteins from conformational change; new results on citrate synthase and T4 lysozyme. Prot. Struct. Funct. Genet. **30:**144–154.
23. **Kragol, G., S. Lovas, G. Varadi, B. A. Condie, R. Hoffmann, and L. Otvos, Jr.** 2001. The antibacterial peptide pyrrhocoricin inhibits the ATPase actions of DnaK and prevents chaperone-assisted protein folding. Biochemistry **40:** 3016–3026.
24. **Kragol G., R. Hoffmann, M. A. Chattergoon, S. Lovas, M. Cudic, P. Bulet, B. A. Condie, K. J. Rosengren, L. J. Montaner, and L. Otvos, Jr.** 2002. Identification of crucial residues for the antibacterial activity of the proline-rich peptide, pyrrhocoricin. Eur. J. Biochem. **269:**4226–4237.
25. **Laufen, T., M. P. Mayer, C. Beisel, D. Klostermeier, A. Mogk, J. Reinstein, and B. Bukau.** 1999. Mechanism of regulation of hsp70 chaperones by DnaJ cochaperones. Proc. Natl. Acad. Sci. USA **96:**5452–5457.
26. **Leslie, A. G. W.** 1992. Recent changes to the MOSFLM package for processing film and image plate data. Jt. CCP4/ESF-EACBM Newsl. Protein Crystallogr., vol. 26.
27. **Li, J., Y. Wu, X. Qian, and B. Sha.** 2006. Crystal structure of yeast Sis1 peptide-binding fragment and Hsp70 Ssa1 C-terminal complex. Biochem. J. **398:**353–360.
28. **Mayer, M., and B. Bukau.** 2005. Hsp70 chaperones: cellular functions and molecular mechanism. Cell Mol. Life Sci. **62:**670–684.
29. **McCarty, J. S., S. Rüdiger, H. J. Schönfeld, J. Schneider-Mergener, K. Nakahigashi, T. Yura, and B. Bukau.** 1996. Regulatory region C of the *E. coli* heat shock transcription factor, sigma32, constitutes a DnaK binding site and is conserved among eubacteria. J. Mol. Biol. **256:**829–837.
30. **McCoy, A. J., R. W Grosse-Kunstleve, L. C. Storoni, and R. J. Read.** 2005. Likelihood-enhanced fast translation functions. Acta Crystallogr. D **61:**458–464.
31. **Montgomery, D. L., R. I. Morimoto, and L. M. Gierasch.** 1999. Mutations in the substrate-binding domain of the *Escherichia coli* 70 kDa molecular chaperone, DnaK, which alter substrate affinity or interdomain coupling. J. Mol. Biol. **286:**915–932.
32. **Moro, F., V. Fernández, and A. Muga.** 2003. Interdomain interaction through helices A and B of DnaK peptide binding domain. FEBS Lett. **533:**119–123.
33. **Moro, F., V. Fernández-Sáiz, and A. Muga.** 2006. The allosteric transition in DnaK probed by infrared difference spectroscopy. Concerted ATP-induced rearrangement of the substrate binding domain. Protein Sci. **15:**223–233.
34. **Otvos, L., Jr., O. Insug, M. E. Rogers, P. J. Consolvo, B. A. Condie, S. Lovas, P. Bulet, and M. Blaszczyk-Thurin.** 2000. Interaction between heat shock proteins and antimicrobial peptides. Biochemistry **39:**14150–14159.
35. **Otvos, L., Jr., K. Bokonyi, I. Varga, B. I. Otvos, R. Hoffmann, H. C. J. Ertl, J. D. Wade, A. M. McManus, D. J. Craik, and P. Bulet.** 2000. Insect peptides with improved protease resistance protect mice against bacterial infection. Protein Sci. **9:**742–749.
36. **Perrakis, A., R. Morris, and V. S. Lamzin.** 1999. Automated protein model building combined with iterative structure refinement. Nat. Struct. Biol. **6:**458–463.
37. **Pflugrath, J. W.** 1999. The finer things in X-ray diffraction data collection. Acta Crystallogr. D **55:**1718–1725.
38. **Pierpaoli, E. V., E. Sandmeier, H.-J. Schönfeld, S. Gisler, and P. Christen.** 1998. Control of the DnaK chaperone cycle by substoichiometric concentrations of the co-chaperones DnaJ and GrpE. J. Biol. Chem. **273:**6643–6649.
39. **Pierpaoli, E. V., S. M. Gisler, and P. Christen.** 1998. Sequence-specific rates of interaction of target peptides with the molecular chaperones DnaK and DnaJ. Biochemistry **37:**16741–16748.
40. **Qian, X., W. Hou, L. Zhengang, and B. Sha.** 2002. Direct interactions between molecular chaperones heat-shock protein (Hsp) 70 and Hsp40: yeast Hsp70 Ssa1 binds the extreme C-terminal region of yeast Hsp40 Sis1. Biochem. J. **361:**27–34.
41. **Read, R. J.** 1986. Improved Fourier coefficients for maps using phases from partial structures with errors. Acta Crystallogr. A **42:**140–149.
42. **Rüdiger, S., A. Buchberger, and B. Bukau.** 1997. Interaction of Hsp70 chaperones with substrates. Nat. Struct. Biol. **4:**342–349.
43. **Rüdiger, S., L. Germeroth, J. Schneider-Mergener, and B. Bukau.** 1997. Substrate specificity of the DnaK chaperone determined by screening cellulose bound peptide libraries. EMBO J. **16:**1501–1507.
44. **Rüdiger, S., J. Schneider-Mergener, and B. Bukau.** 2001. Its substrate specificity characterizes the DnaJ cochaperone as a scanning factor for the DnaK chaperone. EMBO J. **20:**1042–1050.
45. **Shi, L., M. Kataoka, and A. L. Fink.** 1996. Conformational characterization of DnaK and its complexes by small-angle X-ray scattering. Biochemistry **35:**3297–3308.
46. **Slepenkov, S. V., and S. N. Witt.** 2002. Kinetic analysis of interdomain coupling in a lidless variant of the molecular chaperone DnaK: DnaK's lid inhibits transition to the low affinity state. Biochemistry **41:**12224–12235.
47. **Slepenkov, S. V., B. Patchen, K. M. Peterson, and S. N. Witt.** 2003. Importance of the D and E helices of the molecular chaperone DnaK for ATP binding and substrate release. Biochemistry **42:**5867–5876.
48. **Stevens, S. Y., S. Cai, M. Pellecchia, and E. R. Zuiderweg.** 2003. The solution structure of the bacterial Hsp70 chaperone protein domain DnaK(393-507) in complex with the peptide NRLLLTG. Prot. Sci. **12:**2588–2596.
49. **Swain, J. F., E. G. Schulz, and L. M. Gierasch.** 2006. Direct comparison of a stable isolated Hsp70 substrate-binding domain in the empty and substrate-bound states. J. Biol. Chem. **281:**1605–1611.
50. **Swain, J. F., G. Dinler, R. Sivendran, D. L. Montgomery, M. Stotz, and L. M. Gierasch.** 2007. Hsp70 chaperone ligands control domain association via an allosteric mechanism mediated by the interdomain linker. Mol. Cell **26:**27–39.
51. **Vagin, A., and A. Teplyakov.** 1997. MOLREP: an automated program for molecular replacement. J. Appl. Crystallogr. **30:**1022–1025.
52. **Wang, Z. X.** 1995. An exact mathematical expression for describing competitive binding of two different ligands to a protein molecule. FEBS Lett. **360:**111–114.
53. **Wawrzynow, A., and M. Zylicz.** 1995. Divergent effects of ATP on the binding of the DnaK and DnaJ chaperones to each other, or to their various native and denatured protein substrates. J. Biol. Chem. **270:**19300–19306.
54. **Wittung-Stafshede, P., J. Guidry, B. E. Horne, and S. J. Landry.** 2003. The J domain of Hsp40 couples ATP hydrolysis to substrate capture in Hsp70. Biochemistry **42:**4937–4944.
55. **Zhu, X., X. Zhao, W. F. Burkholder, A. Gragerov, C. M. Ogata, M. E. Gottesman, and W. A. Hendrickson.** 1996. Structural analysis of substrate binding by the molecular chaperone DnaK. Science **272:**1606–1614.